

Integration of Google Earth Engine and GIS for monitoring and mapping the spatio-temporal of major air pollutants in Sohag Governorate

Abdel-rahman Abdel-wahed Mustafa

Soil and Water Department, Faculty of Agriculture, Sohag University, Sohag, Egypt

Received: 5 Jan. 2025, Revised: 19 Jan. 2025, Accepted: 2 Feb. 2025 Published online: 1 Apr. 2025

Abstract: The present investigation aims to monitor and mapping the spatiotemporal air quality over Sohag Governorate, Egypt. To do so, remote sensing data sets products from the google earth engine (GEE) were integrated with GIS for mapping the major air pollutants. The annually satellite image data of Sentinel-5P for four major pollutants viz., sulfur dioxide (SO₂), nitrogen dioxide (NO₂), ozone (O₃) and carbon mono (CO) for six years from 2019 to 2024. In the studied period, the CO concentrations varied from 28 to 32 ppm whereas, for O₃, NO₂ and SO₂ ranged from 195 to 209, 101 to 140 and 52 to 490 ppb, respectively. The obtained results suggested that the area under study is suffer from low air quality, which affected both environment and the public health.

Keywords: GEE; GIS; air pollutants; remote sensi

1. Introduction

The major environmental problems facing many cities are air pollution due to increased population, traffic, industry, and agricultural biomass burning events, and natural sources of particulate matter, such as dust and sand events and anthropogenic fuel consumption in transportation and industrial activities [1]. Additionally, high concentrations of many air pollutants can cause serious health problems such as pulmonary and cardiovascular diseases [2]. Egypt is one of the developing countries that face challenges in terms of air pollution [1,3-5]. The most common air pollutants include, but not limited to particulate matter (PM_{2.5}, PM₁₀), sulfur dioxide (SO₂), nitrogen dioxide (NO₂), ozone (O₃), methan (CH₄), formaldehyde (CH₂O) and carbon mono and dioxide (CO, CO₂) [6].

Recently, there has been growing interest in the use of satellite-based remote sensing has emerged as a powerful tool for air quality assessment and monitoring. Remote sensing techniques allow for the collection of data on air pollution over both spatial and temporal patterns, which can provide a more comprehensive understanding of air quality than traditional monitoring methods [7]. This approach has been used in several studies to monitor air pollution in urban areas around the world, including Cairo [1]. The tropospheric monitoring instrument (Sentinel-5P TROPOMI) was utilized for technical purposes to estimate anthropogenic emissions and design air pollution abatement strategies. Atmospheric compounds such as NO₂, SO₂, CO, and CH₂O, which are historically and currently being released in large amounts in industrial and urban areas, are

of particular interest [8]. Google earth engine (GEE) is a free web-based computing platform developed by Google to facilitate geographical information processing [9]. This cloud-based platform controls an “application programming interface” (API) and a related “interactive development environment” (IDE) that support the algorithms, rapid modeling, and visualization [10]. The Google Earth Engine is also the most widely used platform for handling very large repositories of spectral satellite images and other environmental et al., 2023). The use of GEE for various remote sensing applications such as wetland delineation [11-12], LULC extraction [13-15], and crop mapping [16-19] has become prevalent in recent years. Additionally, GEE utilized for air quality monitoring and assessment [20-23]. Therefore, the main objective of the present investigation is to monitor the spatio-temporal analysis of air quality over Sohag Governorate, Egypt in six successive years viz., 2019, 2020, 2021, 2022, 2023 and 2024 by integrating google earth engine (GEE) and GIS. This provides a more detailed and accurate picture of air quality in the study area, which can help to improve public health and environmental outcomes.

2. Experimental

Study site

The study area covers a part (alluvial plain) of Sohag governorate, Egypt which extending from the northern edge of Qena Governorate at latitude 26° 07' N to the southern edge of Assiut Governorate at latitude 26°57' N. It is bounded between longitudes 31°20' and 32°14' E (Fig. 1). The study area belongs to the arid region of North Africa,

which is generally characterized by hot summer and mild winter with low rainfall. Air temperature ranges between 36.5°C (summer) and 15.5°C (Winter), relative humidity ranges between 51% and 61% (Winter), 33% and 41% (Spring), and 35% and 42% (Summer). Rainfall is generally rare and randomly precipitated over the area.

According to the study of Selmy et al. [24], Sohag Governorate mainly includes four classes of different land-uses viz., urban areas (12.3%), water bodies (3.4%), cultivated soils (60.7%) and bare soils (23.6%) as described in table (1).

Table 1: The description of different land-uses of the study area.

Land-uses/Classes	Description
Waterbodies	Nile River, canals, drainage patterns and waste water treatment plants.
Desert lands	Eastern and Western parts of Nile Valley.
Cultivated lands	Cultivated lands in the Nile Valley and Lands under reclamation.
Urban areas	Urban and rural residential, services, commercial, industrial, and roads.

Collect data

In current study, the annually satellite image data of Sentinel-5P for four major pollutants viz., sulfur dioxide (SO₂), nitrogen dioxide (NO₂), ozone (O₃) and carbon mono (CO) products from the GEE. European Space Agency datasets obtained from the Copernicus Sentinel-5 Precursor satellite mission were used as initial data on the content of various pollutants in the atmosphere.

The Sentinel-5 mission consists of a high-resolution spectrometer system that operates within the ultraviolet to shortwave infrared range, utilizing seven distinct spectral bands: UV-1 (270–300 nm), UV-2 (300–370 nm), VIS (370–500 nm), NIR-1 (685–710 nm), NIR-2 (745–773 nm), SWIR-1 (1590–1675 nm), and SWIR-3 (2305–2385 nm). The instrument will be hosted on the MetOp-SG A satellite. To simplify the procedure for obtaining data from the Copernicus Sentinel-5 Precursor satellite (simplification of data processing of netCDF files), the Google Earth Engine (GEE) was used to calculate annual average concentrations of SO₂, NO₂, O₃, CH₄, CH₂O and CO. Comprising a cloud-based computing platform for analyzing and processing large-scale geospatial data, GEE provides a powerful and flexible environment for working with a wide range of remote-sensing, satellite, and other geospatial datasets, including Sentinel-5 Precursor data. One of the key advantages of using GEE for geospatial analysis consists in its ability to efficiently process and analyze huge amounts of data without the need for expensive computing equipment or software. GEE also offers a collaborative environment for sharing data, code, and analysis results with others. The “Sentinel-5P L3” collection was used to estimate the concentration of pollutants (for example, for nitrogendioxide. Image Collection (COPERNICUS/S5P/OFFL/L3_NO₂)). For the collection, various methods of filtering (obtaining average annual and monthly values) and data processing (cropping along the boundaries of the studied area) and further analysis of the resulting raster values of pollutants were used. The categories and corresponding concentrations for the studied pollutants are shown in the table (2) as elaborated by EPA, 2009[25].

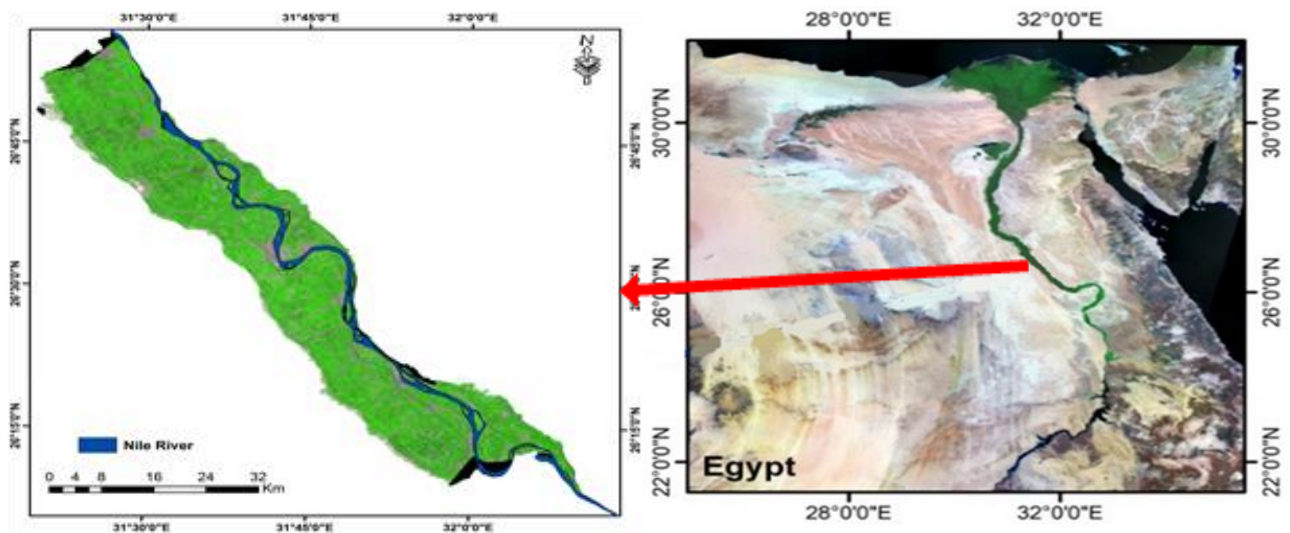


Fig. 1: Location map of the studied area

Table 2: The categories and corresponding concentrations for the studied pollutants

CO (ppm)	O ₃ (ppb)	SO ₂ (ppb)	NO ₂ (ppb)	category
0-4.4	0-54	0-35	0-53	Good
4.5-9.4	55-70	36-75	54-100	Moderate
9.5-124	71-85	76-185	101-360	Unhealthy for sensitive group
12.5-15.4	86-105	186-304	361-649	Unhealthy
15.5-30.4	106-200	305-604	650-1249	Very unhealthy
30.5-50.4	201-604	605-1004	1250-2049	Hazardous

3. Results and discussion:

3.1. Carbon monoxide (CO) concentrations:

Addressing the challenge of CO emission into the atmosphere, through incomplete combustion of compounds such as gasoline, natural gas, oil, coal, and wood in addition to traffic emissions, industrial production, and biomass burning [26]. In the studied period, the CO concentrations varied from 28 to 32 ppm. It was an increase in CO concentrations during 2021 and 2024, whereas, nearly constant concentrations were observed from 2019 until 2022 (figure 2 and table 3). High CO concentration is normally related to locality and population density [27]. In addition, the high CO concentration may be due to the anthropogenic activities as well as the emissions from vehicles and where many power plants and industries are located [28]. The highest concentrations of CO were found around the big cities, main roads and in the south part of the studied area. According to WHO, the CO levels could be described as very unhealthy to hazardous effects.

Table 3: Annual maximum and minimum concentrations of major air pollutants over the study area

Year	CO (ppm)	O ₃ (ppb)	NO ₂ (ppb)	SO ₂ (ppb)
2019	29-31	195-197	104-119	63-438
2020	30-31	201-202	101-118	81-490
2021	30-32	201-203	101-118	64-428
2022	28-29	204-206	107-129	60-416
2023	29-30	201-203	114-137	52-441
2024	30-32	200-209	111-140	57-445

3.2. Ozone (O₃) concentrations:

Ozone is a major greenhouse gas; thus, it plays an important role in both weather and climate, and its impact varies from global to regional scales [29]. While it represents only 0.0012% of the atmospheric composition, ozone acts as an absorber for the energetic particle from the solar ultraviolet radiation (UV), protecting the earth from harmful radiation [30], which has a harmful effect on human health particularly on the skin [31]. The observed increase in UV radiation at the earth's surface has been due to the

decrease of amount of ozone at the stratospheric atmospheric layer [32], which is caused by photochemical losses related to anthropogenic reasons [33-34].

Ozone production results from the photochemical reaction of two primary pollutants viz., NO_x (NO and NO₂) and hydrocarbons from industry, traffic, vegetation, and biomassburning. During the night, ozone is destroyed by NO emitted by local sources and by deposition to the ground.

In the current investigation, the O₃ concentrations during the studied period (table 3 and figure 3) ranged from 195 to 209 ppb. The extremely high concentrations of O₃ in the ambient urban air of the study area as might be anticipated. According to WHO, the levels of O₃ concentration are described as very unhealthy to hazardous categories.

3.3. Nitrogen oxide (NO₂) concentrations:

NO₂ is a toxic air pollutant that causes severe health impacts and premature death, and it is responsible for tens of deaths annually in Cairo, making it a major health risk in urban and industrial areas. The concentrations of NO₂ ranged from 101 to 140 ppb (figure 3), which means that the NO₂ levels varied between unhealthy for sensitive groups. The presence of this pollutant is closely linked to transportation emissions and heating demands this result aligns with the observation of Hereher et al. [1], which explains its higher concentrations in densely populated areas with high population density. The amount of NO₂ in the atmosphere is linked to several emission sources, such as vehicular emissions and natural sources. The highest concentrations were observed nearby the bigger cities such as Tema, Tahta, Gyhena, Sohag and Alminshah.

3.4. Sulfur dioxide (SO₂) concentrations:

SO₂ gas concentrations in the study area's troposphere, it is primarily associated with industrial and power generation facilities and population density. This pattern is particularly noticeable where significant textile, smelting, chemical, petroleum industries, and electricity generation plants are located. These industrial operations predominantly utilize high sulfur heavy fuel, resulting in the emission of SO₂ and making the region a prominent hotspot for SO₂ emissions [22].

While the majority of SO₂ concentration is attributed to emissions from specific industrial activities in the study area, surprisingly, some residential areas also experience relatively high levels of SO₂. The reason behind these unusually high concentrations of SO₂ in the new urban communities is primarily the extensive use of diesel-fueled trucks for constructing new asphalt roads and carrying out construction activities [22]. Accordingly, the annual concentrations of SO₂ during the studied period ranged from 52 to 490 ppb which indicated that the categories varied from moderate to unhealthy as shown in figure (5). As

appears in figure (5), the highest concentration of SO₂ were found around the bigger cities in the study area and heavy populated area.

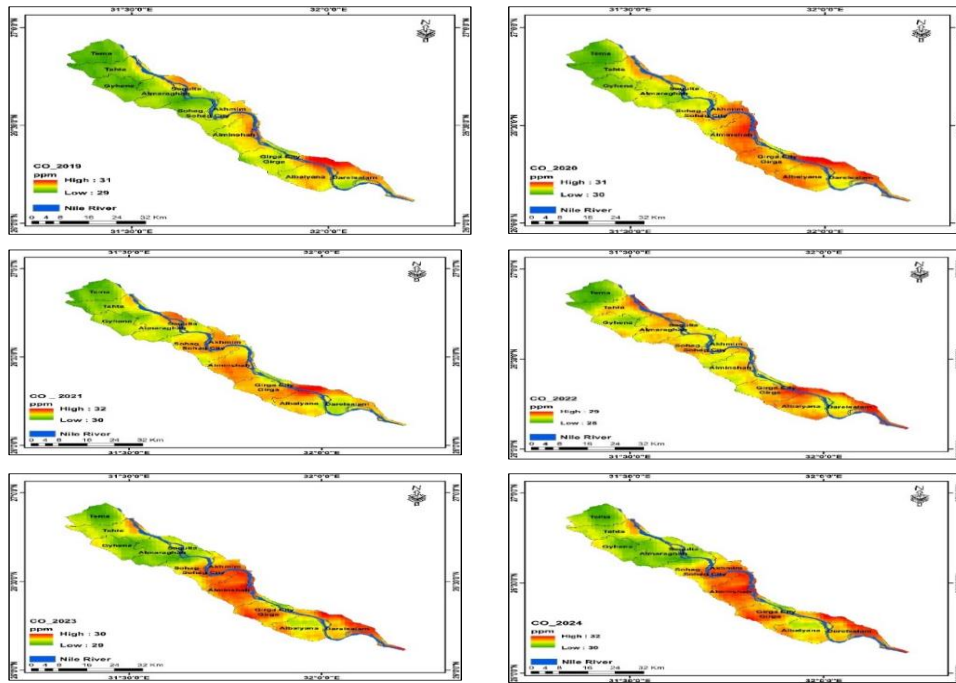


Fig. 2: The distribution of CO in the study area for the period 2019 to 2024.

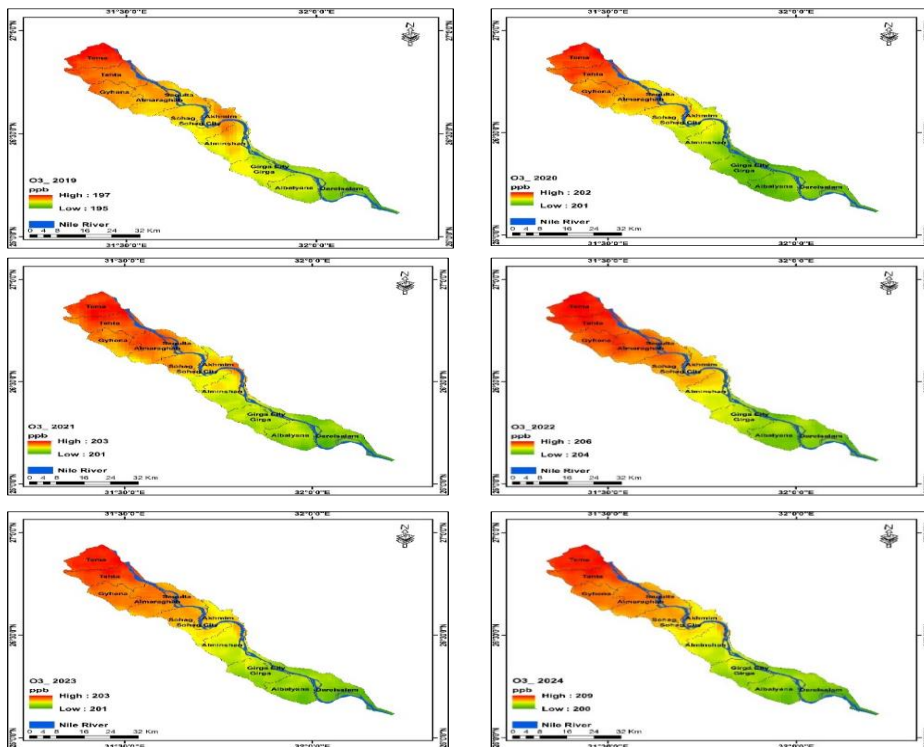


Fig. 3: The distribution of O₃ in the study area for the period 2019 to 2024.

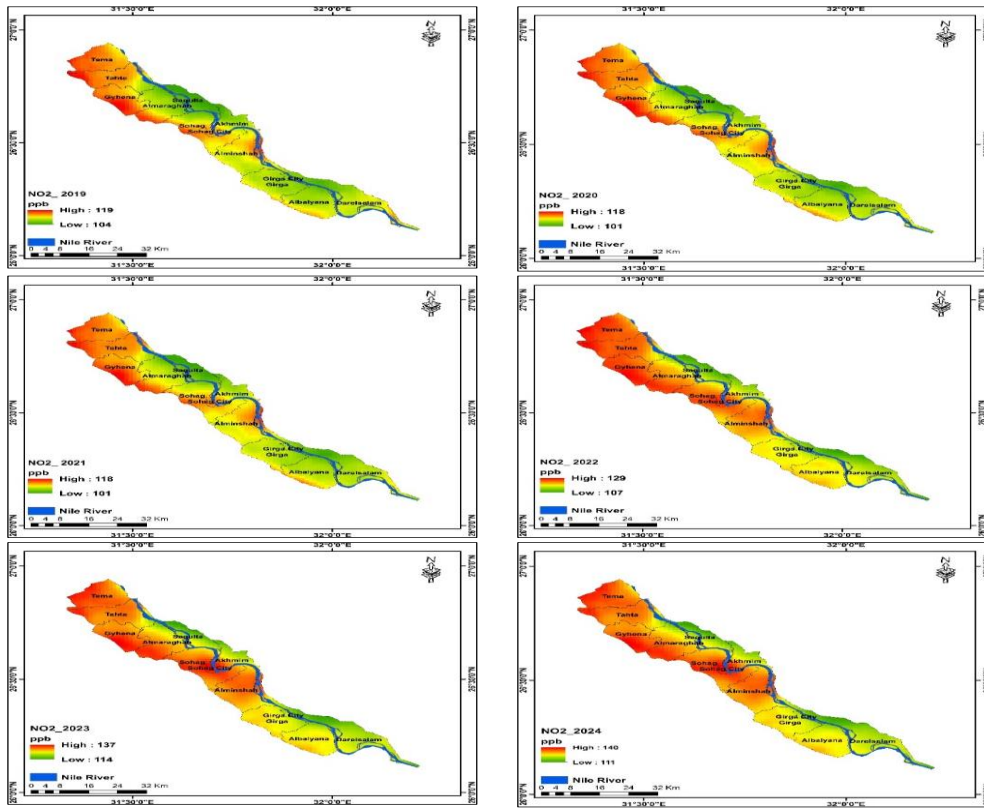


Fig. 4: The distribution of NO₂ in the study area for the period 2019 to 2024.

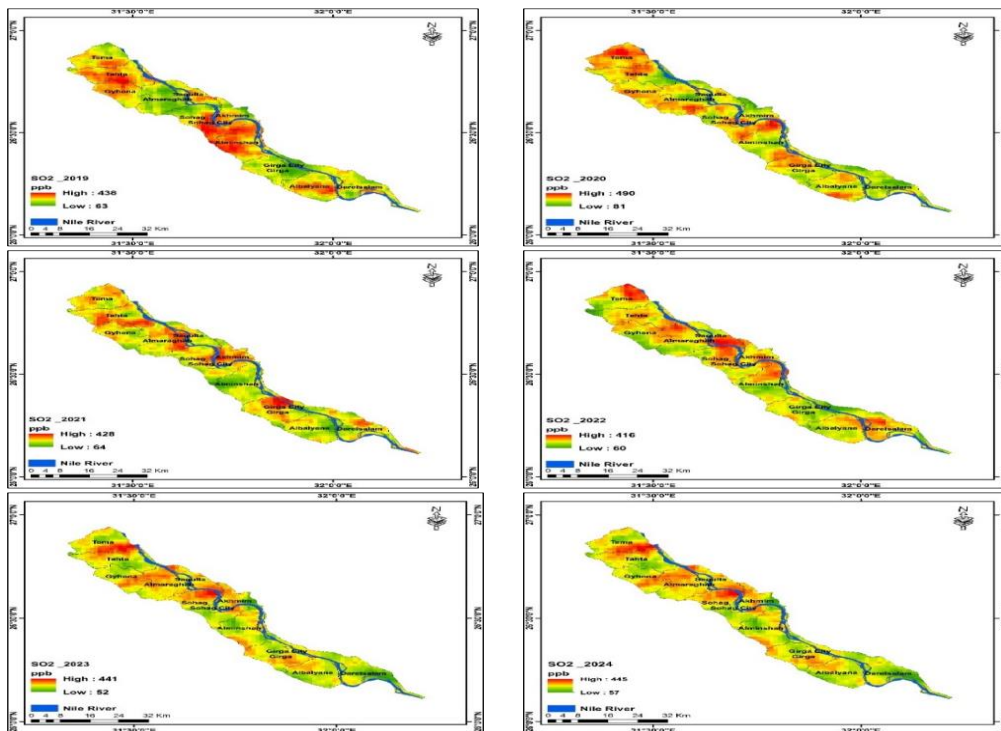


Fig. 5: The distribution of SO₂ in the study area for the period 2019 to 2024.

4. Conclusion

Air pollution represents one of the major environmental stressors with serious implications on human health and ecosystem balance. Recently remote sensing imageries as an alternative cost and time-effective method compared with regular monitoring techniques were used for provision of appropriate data concerning air quality over large areas. In this context, Sentinel-5P satellite provides high-resolution images of atmospheric pollutants including nitrogen dioxide (NO₂), ozone (O₃), carbon monoxide (CO) and sulfur dioxide (SO₂). The obtained results showed high variation in the concentration of CO, O₃, NO₂ and SO₂, in the study area due to the primary sources of air pollution in the study area including basically industry, urbanization and transportation. Furthermore, the results demonstrated that the study area is subjected to high emissions of air pollutants primarily due to industry and traffic. Additionally, the uncontrolled urban expansion of the urban centers causes frequent air pollution issues. The results revealed the excellence of satellites in detection of air pollutants in the study area due to almost daily global coverage. Additionally, the satellite data provides superior spatial distribution of the aerosols, which is considered difficult to measure from ground observations especially during storm events. Furthermore, there is a lack of ground measurements as it is not feasible to put a dense ground monitoring network to assess and monitor surface air quality. Even Though, air pollutants measurements using satellite data have some uncertainty, but satellite data can serve as surrogate to measure the surface level of air quality. Therefore, it is crucial to understand the uncertainties associated with satellite data. We highly recommend that users must pay attention to the quality flags and density of the data for a specific region.

5. References

- [1] M. Hereher, R. Eissa, A. Alqasemi and A.M. El Kenawy, "Assessment of air pollution at Greater Cairo in relation to the spatial variability of surface urban heat island", *Environ. Sci. Pollut. Res.*, vol. 29, 21412-21425, 2022.
<https://doi.org/10.1007/s11356-021-17383-9>.
- [2] H. Wen, H. P. Nie, M. Liu, R. Peng, T. Guo, C. Wang and X. Xie, "Multi-health effects of clean residential heating: evidences from rural China's coal-to-gas/electricity project", *Energy Sustain. Dev.*, vol 73, pp 66-75, 2023.
- [3] M.K. Mostafa, G. Gamal and A. Wafiq, "The impact of COVID19 on air pollution levels and other environmental indicators-A case study of Egypt", *J. Environ. Manag.* Vol.277, pp. 111496, 2021.
- [4] IPCC, 2021. Contribution of Working Groups I, II and III to the Sixth Assessment Report of the Intergovernmental Panel on Climate Change.
<https://www.ipcc.ch/report/ar6/wg1/>.
- [5] Q. Liu, D. Yang and L. Cao, "Evolution and prediction of the coupling coordination degree of production-living-ecological space based on land use dynamics in the daqing river basin", *China. Sustainability*, vol. 14, pp. 10864, 2022.
- [6] F. Nouri, M. Taheri, M. Ziaddini, J. Najafian, K. Rabiei and A. Pourmoghadas, "Effects of sulfur dioxide and particulate matter pollution on hospital admissions for hypertensive cardiovascular disease: a time series analysis", *Front. Physiol.*, vol. 14, pp. 1124967, 2023.
- [7] J. Hwang, K. Maharjan and H. Cho, "A review of hydrogen utilization in power generation and transportation sectors: achievements and future challenges", *Int. J. Hydrogen Energy*, vol. 48 (74), pp. 28629e28648, 2023.
- [8] E.W Nyaga., "Aerosol Remote Sensing and Modelling: Estimation of Vehicular Emission Impact on Air Pollution in Nairobi", University of Nairobi, Kenya, 2021.
- [9] N. Gorelick, M. Hancher, M. Dixon, S. Ilyushchenko, D. Thau, R. Moore, "Google Earth Engine: Planetary-scale geospatial analysis for everyone", *Remote sensing of Environment*, vol. 202, pp. 18-27, 2017.
- [10] P. Pérez-Cutillas, A. Pérez-Navarro, C. Conesa-García, D. A. Zema and J. P. Amado-Álvarez, "What is going on within google earth engine? A systematic review and meta-analysis", *Remote sensing applications: Society and environment*, vol. 29, pp. 100907, 2023.
- [11] M. Amani, B. Brisco, M. Afshar, S. M. Mirmazloumi, S. Mahdavi, S. M. J. Mirzadeh, W. Hung and J. Granger, "A generalized supervised classification scheme to produce provincial wetland inventory maps: An application of Google Earth Engine for big geo data processing", *Big Earth Data*, vol. 3(4), pp. 378-394, 2019.
- [12] M. Mahdianpari, H. Jafarzadeh, J. E. Granger, F. Mohammadimanesh, B. Brisco, B. Salehi, Q and Weng, "A large-scale change monitoring of wetlands using time series Landsat imagery on Google Earth Engine: a case study in Newfoundland", *GIScience & Remote Sensing*, vol. 57(8), pp. 1102-1124, 2020.
<https://doi.org/10.1080/15481603.2020.1846948>.
- [13] H. A. Zurqani, C. J. Post, E. A. Mikhailova, M. A. Schlautman, and J. L. Sharp, "Geospatial analysis of land use change in the Savannah River Basin using Google Earth Engine", *International journal of applied earth observation and geoinformation*, vol. 69, pp. 175-185, 2018.
- [14] A. Ghorbanian, M. Kakooei, M. Amani, S. Mahdavi, A. Mohammadzadeh and M. Hasanlou, "Improved land cover map of Iran using Sentinel imagery within Google Earth Engine and a novel automatic workflow for land

cover classification using migrated training samples”, *ISPRS Journal of Photogrammetry and Remote Sensing*, vol. 167, pp. 276-288, 2020.

- [15] E. A. Abdelsamie, A. R. A. Mustafa, A. S. El-Sorogy, H. F. Maswada, S. A. Almadani, M. S. Shokr and Meroño de Larriva, “Current and Potential Land Use/Land Cover (LULC) Scenarios in Dry Lands Using a CA-Markov Simulation Model and the Classification and Regression Tree (CART) Method: A Cloud-Based Google Earth Engine (GEE) Approach”, *Sustainability*, vol. 16(24), pp. 11130, 2024.
- [16] J. Xiong, P.S. Thenkabail, M.K. Gumma, P. Teluguntla, J. Poehnelt, R.G. Congalton, K. Yadav and D. Thau, “Automated cropland mapping of continental Africa using Google Earth Engine cloud computing”, *ISPRS Journal of Photogrammetry and Remote Sensing*, vol. 126, pp. 225-244, 2017.
- [17] A. J. Oliphant, P. S. Thenkabail, P. Teluguntla, J. Xiong, M. K. Gumma, R. G. Congalton and K. Yadav,” Mapping cropland extent of Southeast and Northeast Asia using multi-year time-series Landsat 30-m data using a random forest classifier on the Google Earth Engine Cloud”, *International Journal of Applied Earth Observation and Geoinformation*, vol. 81, pp. 110-124, 2019.
- [18] S. Xie, L. Liu, X. Zhang, J. Yang, X. Chen and Y. Gao, “Automatic land-cover mapping using landsat time-series data based on google earth engine”, *Remote sensing*, vol. 11(24), pp. 3023, 2019.
- [19] M.K. Gumma, P.S. Thenkabail, P.G. Teluguntla, A. Oliphant, J. Xiong, C. Giri, V. Pyla, S. Dixit and A.M. Whitbread, “Agricultural cropland extent and areas of South Asia derived using Landsat satellite 30-m time-series big-data using random forest machine learning algorithms on the Google Earth Engine cloud”, *GIScience & Remote Sensing*, vol. 57(3), pp.302-322, 2020.
- [20] Y. Meng, M. S. Wong, H. Xing, M. P. Kwan, and Zhu, R.,” Yearly and daily relationship assessment between air pollution and early-stage COVID-19 incidence: Evidence from 231 countries and regions”, *ISPRS International Journal of Geo-Information*, vol. 10(6), pp. 401, 2021.
- [21] F. Ghasempour, A. Sekertekin and S. H. Kutoglu, “Google Earth Engine based spatio-temporal analysis of air pollutants before and during the first wave COVID-19 outbreak over Turkey via remote sensing”, *Journal of Cleaner Production*, vol. 319, pp. 128599, 2021.
- [22] S. Sameh, F. Zarzoura and M. El-Mewafi, “Spatio-temporal Analysis Mapping of Air Quality Monitoring in Cairo using Sentinel-5 satellite data and Google earth engine”, *Mansoura Engineering Journal*, vol. 49(1), pp. 3, 2023.
- [23] B. Halder, I. Ahmadianfar, S. Heddam, Z.H. Mussa, L. Goliatt, M.L. Tan, Z. Sa’adi, Z. Al-Khafaji, N. Al-Ansari, A.H. Jawad, and Z.M. Yaseen,” Machine learning-based country-level annual air pollutants exploration using Sentinel-5P and Google Earth Engine”, *Scientific Reports*, vol. 13(1), pp.7968, 2023.
- [24] S.A. Selmy, D.E. Kucher, G. Mozgeris, A.R. Moursy, R. Jimenez-Ballesta, O.D. Kucher, M.E. Fadi and A. -r.A.J.R. S Mustafa,” Detecting, analyzing, and predicting land use/land cover (LULC) changes in arid regions using landsat images, CA-Markov hybrid model, and GIS techniques”, vol. 15, pp. 5522, 2023.
- [25] EPA (United States Environmental Protection Agency), “Technical assistance document for reporting of daily air quality-the air quality index (AQI)”, EPA-454/B-09-001. U.S., Environmental Protection Agency, North Carolina, 2009.
- [26] T. Borsdorff, H. Hu, O. Hasekamp, R. Sussmann, M. Rettinger, F. Hase, J. Gross, M. Schneider, O. Garcia, W. Stremme, and M. Grutter,” Mapping carbon monoxide pollution from space down to city scales with daily global coverage”, *Atmospheric Measurement Techniques*, vol. 11(10), pp.5507-5518, 2018.
- [27] M. Filonchyk and M. Peterson,” Air quality changes in Shanghai, China, and the surrounding urban agglomeration during the COVID-19 lockdown”, *Journal of Geovisualization and Spatial Analysis*, vol. 4(2), pp. 22, 2020.
- [28] G. Gamal, O. M. Abdeldayem, H. Elattar, S. Hendy, M. E. Gabr and M. K. Mostafa, “Remote sensing surveillance of NO₂, SO₂, CO, and AOD along the Suez Canal Pre-and Post-COVID-19 lockdown periods and during the blockage”, *Sustainability*, vol. 15(12), pp. 9362, 2023.
- [29] M. Rex, R.J.P.von der Salawitch, N.R. Gathen, P. Harris, M. Chipperfield and B. Naujokat,” Arctic ozone loss and climate change”, *Geophys. Res. Lett.*, vol. 31, pp. L04116, 2004. [Google Scholar] [CrossRef].
- [30] D. Alexandris, C. Varotsos, K.Y. Kondratyev and G. Chronopoulos,” On the altitude dependence of solar effective UV”, *Phys. Chem. Earth Part C Sol. Terr. Planet. Sci.*, vol. 24, pp. 515–517, 1999. [Google Scholar] [CrossRef].
- [31] World Health Organization (WHO). Protection Against Exposure to Ultraviolet Radiation; Technical Report WHO/EHG #17; WHO: Geneva, Switzerland, 1995. [Google Scholar].
- [32] V.E. Fioletov, L. McArthur, J.E. Kerr and D.I. Wardle, “Long-term variations of UV-Birradiance over Canada estimated from Brewer observations and derived from ozone and pyranometer measurements”, *J. Geophys. Res.*,

vol. 106, pp. 2307–2309, 2001. [Google Scholar] [CrossRef].

[33] N.R.P. Harris, J. Ancellet, L. Bishop, D.J. Hofmann, J.B. Kerr, R.D. McPeters, W.J. Prendez, J. Randel, B.H. Staehelin and A. Subbaraya, “Trends in stratospheric and free tropospheric ozone”, *J. Geophys. Res.*, vol. 102, pp. 1571–1590, 1997. [Google Scholar] [CrossRef].

[34] World Meteorological Organization (WMO). Scientific Assessment of Ozone Depletion: Global Ozone Research and Monitoring Project; Technical Report 50; WMO: Geneva, Switzerland, 2006. [Google Scholar].
